Applied Radiation and Isotopes 196 (2023) 110726

Contents lists available at ScienceDirect

Applied Radiation and Isotopes

journal homepage: www.elsevier.com/locate/apradiso

Evolution of traceable radon emanation sources from MBq to few Bq

Stefan Röttger [a,*], Annette Röttger [a], Florian Mertes [a], Viacheslav Morosch [a], Tanita Ballé [a], Scott Chambers [b]

[a] Physikalisch-Technische Bundesanstalt (PTB), Bundesallee 100, 38116, Braunschweig, Germany
[b] Australian Nuclear Science and Technology Organisation (ANSTO), New Illawarra Road, Lucas Heights, NSW, 2234, Australia

ARTICLE INFO

Keywords:
Radon
Radium
Emanation
Silicon detector
Primary standard

ABSTRACT

In the framework of the EMPIR project traceRadon, stable atmospheres with low-level radon activity concentrations have to be produced for calibrating radon detectors designed to measure outdoor air activity concentrations. The traceable calibration of these detectors at very low activity concentrations is of special interest to the radiation protection, climate observation, and atmospheric research communities.

Radiation protection networks (such as the EUropean Radiological Data Exchange Platform (EURDEP)) and atmospheric monitoring networks (such as the Integrated Carbon Observation System (ICOS)) need reliable and accurate radon activity concentration measurements for a variety of reasons, including: the identification of Radon Priority Areas (RPA); improving the sensitivity and reliability of radiological emergency early warning systems (Melintescu et al., 2018); for more reliable application of the Radon Tracer Method (RTM) to estimate greenhouse gas (GHG) emissions; for improved global "baseline" monitoring of changing GHG concentrations and quantification of regional pollution transport (Chambers et al., 2016), (Chambers et al., 2018); and for evaluating mixing and transport parameterisations in regional or global chemical transport models (CTMs) (Zhang et al., 2021), (Chambers et al., 2019).

To achieve this goal, low activity sources of radium with a variety of characteristics were produced using different methods. Sources ranging from MBq ^{226}Ra down to several Bq ^{226}Ra were developed and characterised during the evolution of production methods, and uncertainties below 2 % (k= 1) were achieved through dedicated detection techniques, even for the lowest activity sources. The uncertainty of the lowest activity sources was improved using a new online measurement technique for which the source and detector were combined in the same device. This Integrated Radon Source Detector device, henceforth an IRSD, reaches a counting efficiency approaching 50 % through detection under quasi 2π sr solid-angle. At the time of this study the IRSD was already produced with ^{226}Ra activities between 2 Bq and 440 Bq.

To compare the working performance of the developed sources (i.e., to establish a reference atmosphere), study the stability of the sources, and to establish traceability to national standards, an intercomparison exercise was carried out at the PTB facility. Here we present the various source production techniques, the determination of their radium activity, and determination of their radon emanation (including assigned uncertainties). This includes details of the implementation of the intercomparison set-up, and a discussion of the results of the source characterisations.

1. Introduction

Radon is, at naturally occurring densities, an invisible, odourless, and chemically inert radioactive noble gas that occurs almost everywhere in varying concentrations of activity. ^{222}Rn is a progeny of the long-lived ^{226}Ra (half-life of about 1600 years), which is ubiquitous in most rock, water, and soil (Commission and Centre, 2020). Like all radioactive substances, radon decays into other elements, emitting radiation, mainly in the form of α-particles. It has been scientifically proven that radon is responsible for the majority of the lung cancer risk in the non-smoking population due to its daughter products (Darby et al., 2005), since inhaled radon progeny can cause significant damage to respiratory cells. In buildings, activity concentrations of radon and its daughter products can reach levels high enough to pose a serious health

* Corresponding author.
E-mail address: Stefan.Roettger@PTB.de (S. Röttger).

https://doi.org/10.1016/j.apradiso.2023.110726
Received 31 May 2022; Received in revised form 19 January 2023; Accepted 14 February 2023
Available online 24 February 2023
0969-8043/© 2023 The Authors. Published by Elsevier Ltd. This is an open access article under the CC BY license (http://creativecommons.org/licenses/by/4.0/).

risk. The higher the radon activity concentration, the greater the health risk: it is estimated that exposure to radon in dwellings is responsible for about 20000 lung cancer related deaths annually in the European Union alone (Angell, 2009). For this reason, more and more regulations are being issued to reduce exposure to radon. The most important document for Europe in this regard is the European DIRECTIVE 2013/59/EURATOM (EBSS, 2013), which is implemented nationally; in Germany, for example, by the Radiation Protection Act (Strahlenschutzgesetz, 2017).

Globally, there is a lack of reliable data on radon activity concentrations in outdoor environments.[1] Since contemporary measurement data mostly lacks the necessary quality, routine measurement simply does not make sense. Instead, questions of radiation protection have relied on indoor measurements of activity concentration, which usually have significantly higher values and are therefore easier to measure. A prerequisite for the creation of reliable data on radon activity concentration in the outdoor environment is a new metrological basis: the traceability of such measurements to the SI system. The implementation of a quality assurance system with valid information about uncertainties is a prerequisite for the comparability of results between such environmental measurements. The basis for this is the existence of available and suitable radon activity standards. This paper provides an overview of some new developments in this field.

2. Radon gas standards and their limitations

The metrology of ^{222}Rn with respect to the dissemination of the unit of activity concentration in Bq·m^{-3} can be fundamentally divided into two different approaches. The first way to quantify radon in an absolute sense is the method of Picolo (1996), in which gaseous radon from the decay of radium (^{226}Ra) is frozen out on a cold point under vacuum. Alpha particles emitted by the solid radon are measured at a defined solid angle such that the unit of activity can be traced back to the base units of seconds and meters. The solid radon can then be returned to the gas phase and can subsequently be used to produce atmospheres of known activity concentration in a defined volume. The activity concentration of an atmosphere produced in this way decreases exponentially with a half-life of about 3.8 days, limiting the counting statistics and hence the achievable uncertainty in the calibration of detectors under test. Consequently, this approach is not suitable for the representation of reference atmospheres with activity concentrations comparable to those typical in the outdoor atmosphere (<100 Bq·m^{-3}). The second way is to use sources containing ^{226}Ra that are designed in such a way that part of the ^{222}Rn produced by ^{226}Ra decay is continuously released into a reference volume, as described in the following section.

3. Radon emanation source types and their traceability

Radon emanation sources continuously replace the radon in the reference volume that is decaying, resulting in a state of equilibrium, (i.e., a constant activity concentration) after about five to ten half-lives (Mertes et al., 2019). Some types of radon emanating sources produced at PTB are depicted in Fig. 1. With exception of type (A), these sources can be characterised using defined solid angle α-spectrometry (DSA) as a primary method to assure the traceability to the SI. Source type (B) to (F) are therefore regarded as primary and discussed in more detail. Source type (F) is furthermore a class of its own since it is a combination of a source and a detector in one device. A so-called Integrated Radon Source Detector (IRSD). Features of the IRSD are demonstrated separately. For the type (A) sources the amount of radium solution and its activity concentration have to be traceable measured and transferred quantitatively to the source, because the α-particles

[1] More general, the „activity concentration in outdoor environments“ is regarded as a lower activity concentration as in usual buildings. Recent measurements indicate values in the range of 0.1 Bq·m^{-3} to 100 Bq·m^{-3}.

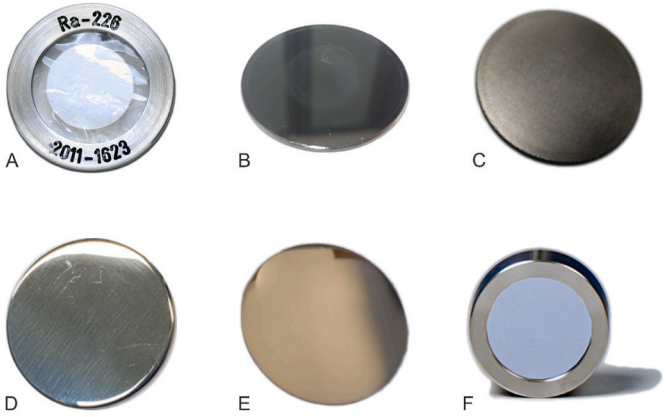

Fig. 1. Overview of radon emanation sources. Historical development from upper-left to lower-right.
(A) ^{226}Ra solution drop-cast to fibre filter enclosed between polyethylene foils.
(B) ^{226}Ra solution electrodeposit to a stainless steel backing.
(C) Mass separated ion-implanted ^{226}Ra onto a tungsten backing (W or Al).
(D) thermal physical vapor deposition of $^{226}RaCl_2$ onto stainless steel backing.
(E) thermal physical vapor deposition of $^{226}RaCl_2$ onto a 1″ diameter silicon wafer.
(F) thermal physical vapor deposition of $^{226}RaCl_2$ onto 450 mm^2 ion-implanted silicon detector.

from radioactive decay of the ^{226}Ra are not able to leave the source, which separates their way of traceability from the other sources. Due to the dependency of the source type (A) to environmental parameters, their characterisation is difficult and restricted to specified environments, but it can provide high radon emanation rates, depending on the polyethylene foil with a large spread of values. Type (B) sources which still contain some impurities from the solution on its surface, also show dependency on environmental parameters but already with reduced significance. The least dependence possible is reached with type (C) sources where only mass separated ^{226}Ra is at the surface. Thermal physical vapor depositioned sources (D-F) are getting close to this behaviour. Therefore, some characteristics of this source type are listed in Table 1.

4. Primary radon emanation standards

Unlike thoron emanating thorium sources, which can be produced in an electrolytic process, radon emanating sources cannot be produced this way, because of its small electronegativity. Having a carrier free solution of radium available, electrodeposition to a stainless-steel backing is feasible. At the PTB lab sources of type (B) have been produced, characterised, and used, with a range of the radium activity A (^{226}Ra) from about 40 Bq to 700 Bq.

Table 1
List of type (A) drop cast radon emanation sources (according to Fig. 1) with their main characteristics determined via γ-spectrometry using HPGe detector. The stable emanation coefficient is indicated as η. The activity concentration (C) given is for a reference volume of 500 L. The assigned uncertainties are indicated with an expansion factor of k=1.

Source number	$A(226Ra)$ Bq	χ			C Bq·m^{-3}		
2011–1775	113	0.685	±	0.012	152	±	4
2011–1585	210	0.158	±	0.014	65	±	6
2011–1777	214	0.870	±	0.002	365	±	5
2011–1816	273	0.059	±	0.009	32	±	5
2011–1624	512	0.684	±	0.003	686	±	9
2011–1817	788	0.761	±	0.005	1172	±	16
2011–1623	883	0.759	±	0.002	1314	±	16
2011–1671	1315	0.728	±	0.011	1870	±	34

For the first time, the characterisation of these source is not only possible from characterised solution applying weighing and quantitative transfer or γ-spectrometry, but with α-spectrometry under defined solid angle (DSA), which is a primary, standard method for the determination of the activity of α emitting nuclides. A schematic setup of a DSA measurement is shown in Fig. 2.

The characterisation of the emanation of a source is determined by the disequilibrium of the source nuclide and its progeny, as described in Mertes et al. (2019), Röttger et al. (2001), Linzmaier and Röttger (2013, 2014). This difference technique is applied using the results of γ-spectrometric measurements and full energy peak analysis. Fig. 3 illustrates the schematic setup of a classical emanation measurement with two γ-radiation sensitive detectors. A $LaBr_3$ detector (alternative $CeBr_3$) as a scintillation detector that is light weight, with sufficient efficiency and energy resolution for portable applications and a HPGe semiconductor detector with better energy resolution for application in a lab. Operation in a closed, well defined volume, a sufficient air exchange between source volume and calibration atmosphere volume has to be guaranteed. In case of an open flow calibration system, the volume of the air flow through the source volume has to be traceably characterised, for instance using a calibrated mass flow controller.

These kind of source measurement setups are well suited for stable, conditions available in a lab, but might suffer varying emanation in case of outdoor environmental application in field.

To distinguish between source internal effects and calibration uncertainties, very clean and isotopically pure emanation sources have been produced on tungsten and aluminium backings from a carrier free ^{226}Ra solution using thermal, laser resonance ionisation followed by accelerator mass separation and ion-implantation (Mertes et al., 2022a) at the RISIKO mass separator. A list of sources produced with their characteristic values determined by γ- and α-spectrometry are given in Table 2. Where $A_{\alpha\text{-}DSA}$ represents the absolute ^{226}Ra activity implanted in the source and $\varepsilon_{\alpha\text{-}DSA}$ its respective production efficiency[2] (both determined by DAS α-spectrometry). χ_α the emanation efficiency of the source determined with α-spectrometry. χ_γ for γ-spectrometry respectively. Good agreement within the uncertainties is observed. *FWHM* ^{226}*Ra* shows the full width at half maximum energy resolution in the α-spectrometry at 4784 keV for the ^{226}Ra α-emission, which is close to the energy resolution of the ion-implanted silicon detector in use and pronounces the high quality of this sources.

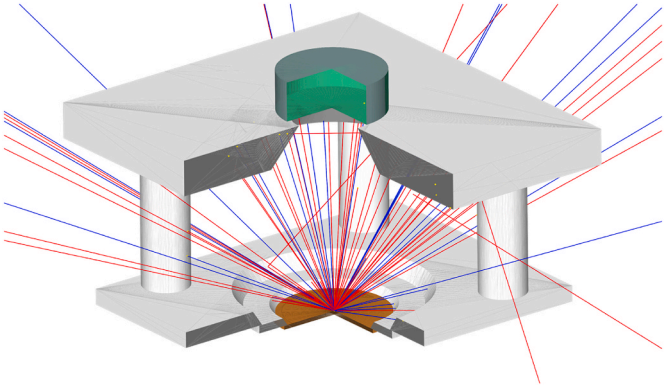

Fig. 2. Simulation of the defined solid angle **α**-spectrometry setup, to determine the activity of a α-particle emitting nuclides. Shown is the ion-implanted silicon detector for the α-particles on top of the solid angle defining aperture system and the α-source, respectively the IRSD system below.

[2] Where production efficiency denotes the ratio of the amount of ^{226}Ra used for production of the source, compared to the amount of ^{226}Ra available on the source after production.

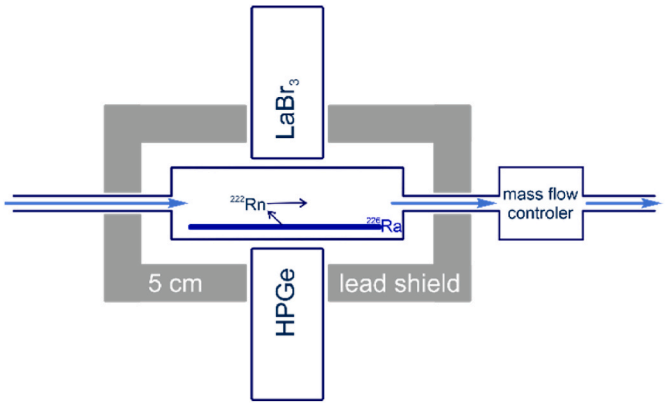

Fig. 3. Schematic view of the measurement setup to determine the emanation of a ^{226}Ra emanation source quasi online applying γ-spectrometric detectors e. g. HPGe or $LaBr_3$ detector.

Table 2
Overview of the available mass separated ion-implanted radon emanation sources with their measured characteristic parameters.

Target (Material)	$A_{\alpha\text{-}DSA}$ Bq	$\varepsilon_{\alpha\text{-}DSA}$ %	χ_α	χ_γ	*FWHM* ^{226}*Ra* keV
2018-1120 (W)	766 ± 77	30 ± 3	0.308 ± 0.004	0.3077 ± 0.0029	16.5
2018-1121 (W)	1155 ± 115	60 ± 6	0.340 ± 0.004	0.341 ± 0.005	16.8
2018-1122 (W)	724 ± 72	32 ± 3	0.285 ± 0.004		17.1
2018-1133 (Al)	798 ± 80	32 ± 3	0.273 ± 0.004	0.272 ± 0.004	15.3
2018-1134 (Al)	513 ± 51	46 ± 5	0.260 ± 0.003		15.5
2018-1128 (Al)	475 ± 47	46 ± 5	0.233 ± 0.004	0.230 ± 0.004	16.0

The high metrological quality of this type of sources is not only visible in the small energy resolution values (*FWHM* ^{226}*Ra*, which is less than 10 % wider than the resolution of the detector specified by the manufacturer) in Table 2 but is also proven by the neglectable dependency from environmental parameter changes. As an example, the normalised ration between the full energy peak areas of the main transitions from ^{214}Pb and ^{226}Ra ($R(^{214}Pb)/R(^{226}Ra)$), which represent the emanation of the source, are plotted in parallel to the relative humidity (φ) of the source surrounding air in Fig. 4. Even though the relative humidity was changed very rapidly from about 12 %rH to about 75 %rH, no change in the peak area ratio aside from statistical fluctuations can be observed.

The ^{226}Ra activity range from about 450 Bq to 1200 Bq, the excellent energy resolution and the absence of impurities make these sources the ideal sources for fundamental investigation of the emanation behaviour and as well as calibration sources for primary calibrations. Even the build up of the progeny and their recoil displacement can be observed. On the other hand, the production possibilities are very rare (RISIKO (Mertes et al., 2022a), (Kieck et al., 2019), Isolde (Jörg et al., 2022), (Catherall et al., 2017)) which makes them very precious and not suitable for in field calibrations or services.

To overcome the disadvantages of the production of the ion-implanted sources and keep their advantages, PTB started the development of a new source production technique. The technique of choice is thermal, physical vapor deposition (tPVD). $^{226}RaCl_2$ is produced from PTB radium standard solution as described in (Mertes et al., 2022b). A small vacuum chamber with electrical, ohmic heating and dedicated aperture system is used for the tPVD and sources on stainless steel discs

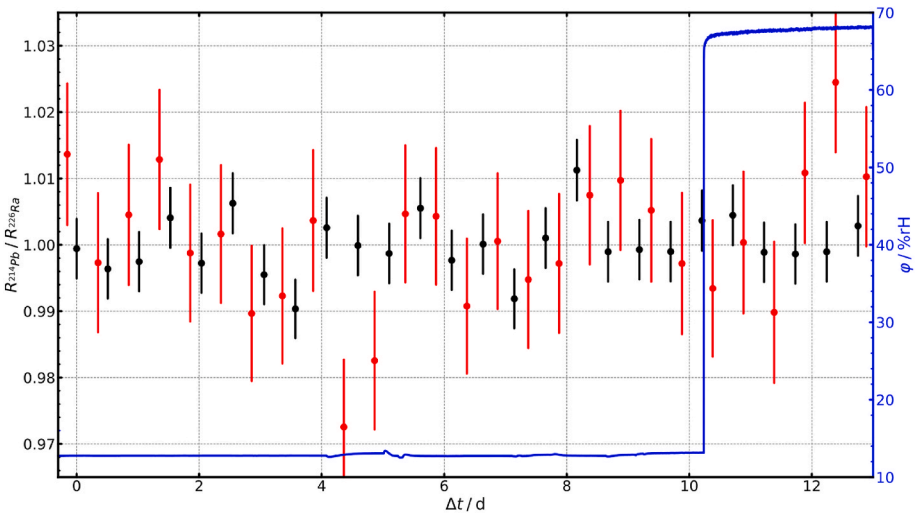

Fig. 4. Determination of the time resolved emanation of a ^{226}Ra emanation source applying the γ-spectrometry method (ratio of full energy peak areas of ^{214}Pb (352 keV) and ^{226}Ra (186 keV), red: 1.5″ $LaBr_3$, black: HPGe) and the relative humidity φ (blue). No dependence is found within the statistical uncertainty.

and standard 1" silicon wafers are produced and characterised.

5. Active primary radon emanation standards

With a slightly modified tPVD setup it is possible, to use an ion-implanted silicon detector as backing for the deposition of the ^{226}Ra. With the operation of the detector after the deposition of the ^{226}Ra on its surface, it operates as an IRSD. With such a device it is possible to follow the emanation of the source quasi on-line, which makes it a perfect device to produce traceable ^{222}Rn atmospheres with outdoor ^{222}Rn activity concentrations and under changing outdoor environmental conditions. This is one goal of a European metrology project in the framework of EMPIR named traceRadon (19ENV01 (Röttger et al., 2022a),).

Several of these IRSD have been produced at PTB. The main characteristic values are given in Table 3. Beside the specification of the ion-implanted silicon detector used, the amount of deposited ^{226}Ra is given ($A(^{226}Ra)$), as well as its α-detection efficiency with the IRSD device itself ($\varepsilon_{P\alpha\text{-}226}$). This high efficiency is determined through the use of the DSA α-spectrometry at the primary reference standard for α-emitting sources at the national metrology laboratory of Germany (PTB) and therefore traceable to the SI. As an example of such a calibration, a comparison of the α-energy spectra of a primary DSA α-spectrometer and an IRSD measured at the same time in the same vacuum chamber is shown in Fig. 5. Obviously, the resolution of the IRSD is less than of the DSA. This is caused by the large solid angle from the ^{226}Ra to the IRSD detector, which allows for straggling of the α-particles in the dead layer of the detector. On the other hand, the quality of the IRSD as a source becomes visible through the resolution of the DSA α-spectrum, which is close to the electronic resolution of the detector itself. The recoil displacement of the progeny of ^{226}Ra is visible through the double peak structure for instance at ^{222}Rn, ^{218}Po or ^{214}Po. The explanation of this structure could though not fully be resolved and will be part of further, detailed investigations (Marouli et al., 2017).

The analysis of the IRSD signals with the resulting peak areas are understood well and can be fitted and deconvoluted very accurately, see Fig. 6 (Mertes et al., 2019).

Using the so determined peak areas as time resolved information is feasible, since the efficiency of the IRSD with approx. 50 % is very high. Having the time resolved information about the ratios between ^{226}Ra and its progeny, we can regard the IRSD system as a well-known radioactive decay system. When this system is modelled, it is capable to be approximated in a recursive Bayesian estimation as a switching linear dynamical system. Which allows to absolutely follow the emanation of ^{222}Rn from the IRSD by itself.

Examples of such an emanation trace are show in Fig. 7 and Fig. 8. Within these figures, the grey dots represent the determined time resolved peak areas of ^{222}Rn (top graph, $N(^{222}Rn)$) and ^{226}Ra (second graph from top, $N(^{226}Ra)$). The blue curves in the upper three graphs represent the results of the estimation algorithm, with respect to the left axis, giving from the top, the ^{222}Rn activity $A(^{222}Rn)$, the ^{226}Ra activity $A(^{226}Ra)$ and the ^{222}Rn emanation η in absolute units of atoms per second. Changes of the inferred emanation η before the change of the humidity occurred are caused by limitations of the inference approach, caused by smoothness constraint on the functional form of η. In both figures a clear change in emanation and a following stabilisation in emanation is visible, which is not so obvious regarding the activity results for ^{222}Rn. The reason for the change is given in the lowest graph of each figure, which shows the relative humidity φ of the air at the IRSD surface. In Fig. 7 the reduction of the relative humidity φ leads to a reduction in the emanation of ^{222}Rn from the source at day 82 of this measurement. The filtered absolute emanation values η reflect this change in quite short time and arrive at stable emanation values within several hours, while the ^{222}Rn activity in the source is still changing after several days. The explanation of this effect is the nature of the radioactive decay. The detection of the ^{226}Ra decay product ^{222}Rn can only occur after the build up through the decay of the ^{226}Ra. So to speak the missing ^{222}Rn has to be build up first. A similar effect is given in Fig. 8 but starting with lower relative humidity and increasing it up to 85 %rH.

Table 3
List of available active radon emanating sources of the IRSD type (F) (according to Fig. 1), with characteristic values (uncertainties assigned are with expansion factor k=1). The detection efficiency $\varepsilon_{P\alpha\text{-}226}$ is determined from the ^{226}Ra count rate compared to its activity. The observed mean η is not an emanation coefficient but an absolute number of emanated ^{222}Rn atoms per second.

Detector Type	Active Area/ Depletion Depth	$A(^{226}Ra)$ Bq	$\varepsilon_{P\alpha-226}$	*observed mean* η s^{-1}
Mirion PIPS®	450 mm^2/300 µm	1.91 ± 0.02	0.502 ± 0.006	0.999 ± 0.017
Ametek Ortec ULTRA®	450 mm^2/300 µm	66.4 ± 0.5	0.494 ± 0.004	see example Fig. 7
Mirion PIPS®	450 mm^2/300 µm	158.6 ± 1.7	0.494 ± 0.005	see example Fig. 8
Mirion PIPS®	450 mm^2/100 µm	442 ± 4	0.492 ± 0.005	209 ± 4

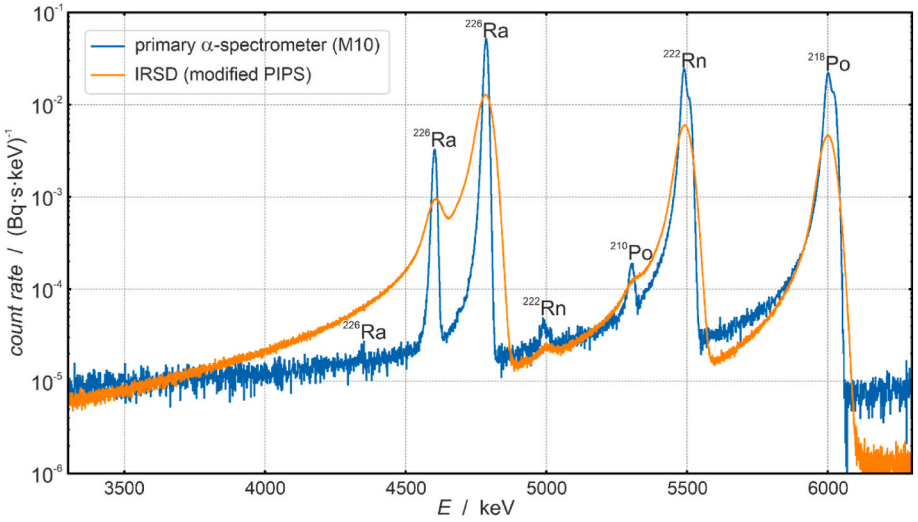

Fig. 5. Absolute α-particle count rate energy spectra, recorded with the primary α-spectrometer of PTB (M10, traceable to the SI) and an IRSD (modified PIPS) at the same time in the same setup. The resolution of the IRSD is less (FWHM is larger) and the count rate is higher as for the M10, because of the much larger solid angle of detection regarding the ^{226}Ra source.

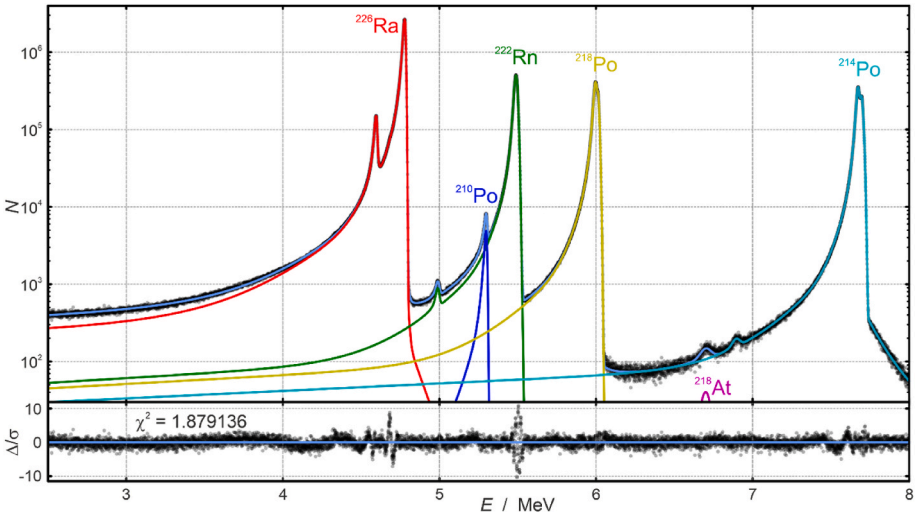

Fig. 6. α-particle energy spectrum of an active IRSD with approximately 440 Bq of ^{226}Ra deposited on an ion-implanted Si-detector (100 µm depletion depth, 450 mm^2 active area), recorded for 5·10^5 s. The black dots mark the events recorded at the specific α-energy. The coloured lines indicate the fitted model, determined for the different α-emitting radio nuclides and the total sum, of which the residual to the data is given in the lower graph.

Here, two effects can be observed. A sudden release of ^{222}Rn at day 30 is visible in the measurement through the peak shape structure in the emanation η and the steep slope in the ^{222}Rn activity. This might be caused by condensation of water on the source surface and solution of radon. And as the second effect the stabilisation of the emanation η right after, which is represented in a slowly decreasing ^{222}Rn activity in the IRSD source.

An overview on the complete uncertainty budget for these measurements with the IRSD is presented in Table 4. The dominant relative contributions are due to the solid angle and ^{226}Ra rates in the DSA α-spectrometer. The solid angle contribution will be improved through a better determination of the IRSD detector surface in a future DSA setup and the DSA statistics could be reduced through a larger detector surface and longer calibration measurement times in the DSA α-spectrometer. An assigned uncertainty below 1 % seams achievable.

6. Radon activity concentration calibration in the lab

At PTB passive and active radon emanation sources have been developed that allow for calibration in closed reference calibration chambers to calibrate outdoor radon activity monitors at radon activity concentrations as low as 10 Bq·m^{-3} with uncertainties well below 10 % (k=1).

This has never been possible in this defined way with other calibration sources before. Only through the development of traceable ^{222}Rn emanation sources which are traceable to the SI, with respect to their ^{226}Ra content as well as their ^{222}Rn emanation and which can be produced with the appropriate, absolute small amounts of ^{222}Rn emanation. With these sources the calibration of outdoor environmental radon detectors, traceable to the SI become feasible and therefore the comparability of outdoor radon measurements as needed for e.g. climate change observation. The first application of these sources in this respect is given as an example with the characterisation of a possible transfer standard detector, the ANSTO 200 L.

In the scope of the traceRadon project the ANSTO 200 L was identified as a possible transfer standard for the traceability chain in environmental radon activity concentration, e.g. the transfer from lab to field. The step forward in well established detection principles for

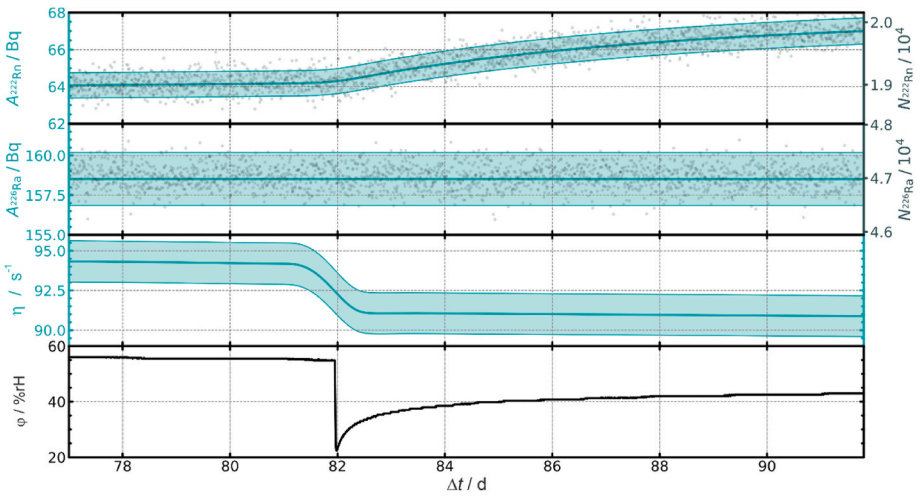

Fig. 7. Quasi online calculation of the emanation of an IRSD reaction to a sudden drop in relative humidity. η indicates the number of ^{222}Rn atoms that are released from the source per second.

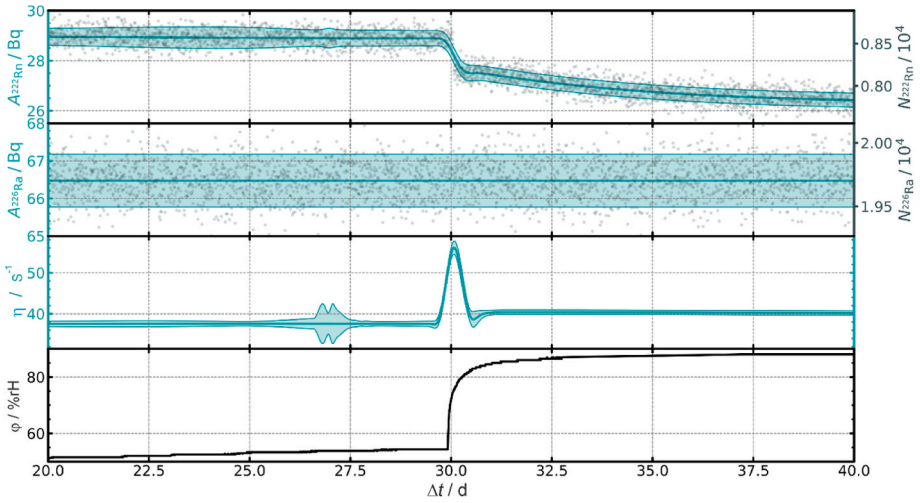

Fig. 8. Quasi online calculation of the emanation of an IRSD reaction to a steep increase in humidity followed by a slow drop of the relative humidity. η indicates the number of ^{222}Rn atoms that are released from the source per second (Röttger et al., 2022b).

Table 4
Full uncertainty budget of a typical IRSD type radon emanation source (uncertainties assigned are with expansion factor k=1). Main contributions of uncertainty, which are going to be improved, are due to the solid angle determination and the statistics of the ^{226}Ra activity determination using the DSA technique.

Description and type	*Value and uncertainty*	*Rel. uncertainty*	*Rel. contribution*
Solid angle (systematic)	(0.00940 ± 0.00006) 4π sr	0.6%	28.4%
Backscattering DSA (systematic)	1 ± 0.002	0.2%	3%
Tailing DSA (systematic)	1 ± 0.003	0.3%	6.7%
Tailing Si (systematic)	1 ± 0.003	0.3%	6.7%
^{226}Ra rate DSA (stochastic)	(0.01796 ± 0.00015) s-1	0.8%	55.1%
^{226}Ra rate Si (stochastic)	(0.9595 ± 0.0004) s-1	0.04%	0.1%
$\varepsilon_{P\alpha\text{-}226}$	0.502 ± 0.006	1.2%	

radiation protection issues is given in Fig. 9 by the comparison of the readings of the ANSTO 200 L and different types of AlphaGUARDs.

The calibration of the ANSTO 200 L measuring device is carried out using ^{222}Rn emanation sources with known very low ^{226}Ra activity and stable emanation coefficients χ inside a closed calibration chamber of volume V. Usually, the activity concentration inside of the calibration chamber for using this method is derived theoretically and compared with the reading from the device at the respective time t, or by regressing it onto the observed readings of the device.

In environmental measurements, the characteristic limits are very important, and they are highly dependent on the intrinsic background. Consequently, great care on the determination of the intrinsic background has been taken. Nevertheless, the intrinsic background does not influence the sensitivity (and the calibration factor) much.

The fit given in Fig. 10 results from four activity concentration levels generated from different emanation sources of type (C) described in Fig. 1. From this, the calibration factor, the sensitivity and the intrinsic background reading are obtained. In addition, the intrinsic background was measured by flushing with aged, synthetic radon free air. A consistency check was performed by the use of a charcoal trap for the air of the radon reference chamber and by closing the in- and out-let of the

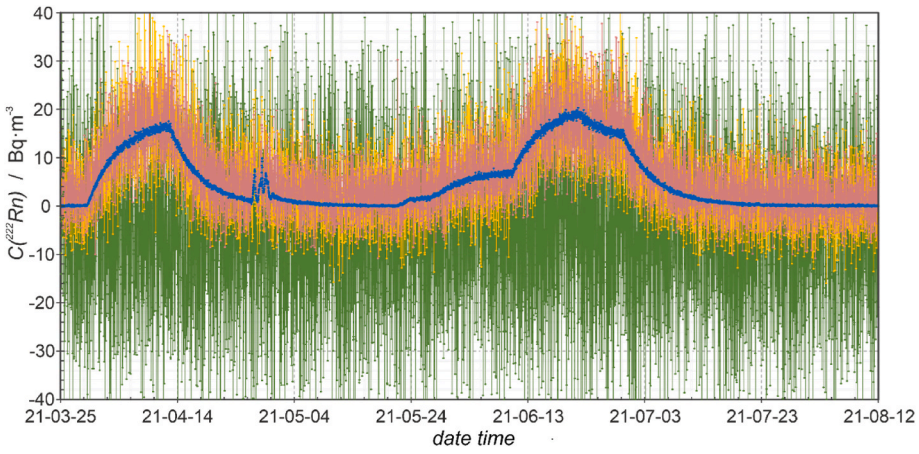

Fig. 9. Low-level radon activity concentration calibration run, with several commercial radon detectors and possible transfer standard for outdoor radon activity concentration levels. All measurement points indicate a 30 min averaged value of ^{222}Rn activity concentration in Bq·m^{-3}. Green shows the measurements of an AlphaGUARD placed outside the calibration chamber in the climate-controlled room, measuring the surrounding environment of the calibration chamber. No significant trends or leakages from the calibration chamber are observed. Yellow and red points display the measurement results, also from AlphaGUARD detectors, inside the calibration atmosphere. The effect of the changing radon activity concentration in the calibration atmosphere is visible, but the statistical fluctuations are often in the same order or even larger than the value itself, even for 30 min integrated values. The measurement results of a possible outdoor activity concentration transfer standard developed with the traceRadon project by ANSTO, the ANSTO 200 L detector, are presented in blue. The details of the calibration of this detector are shown in Fig. 10 (Röttger et al., 2023).

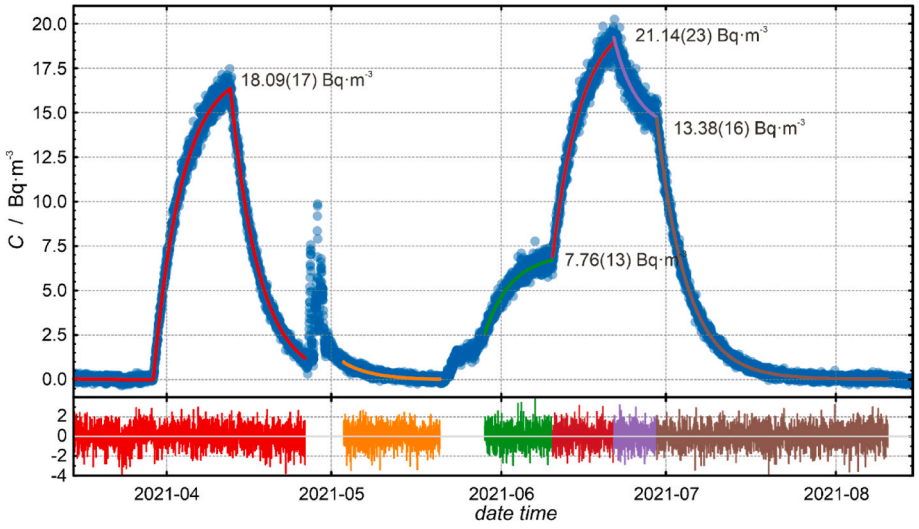

Fig. 10. Calibration of a high-sensitive radon detector (ANSTO 200 L) using different, well characterised radon emanation sources in a large volume climate chamber with traceable volume. Three different radon emanating calibration sources have been used in different combinations during this calibration run, indicated by the different colours in the figure. The y-axis presents the calibrated activity concentration C, detected by the detector. The respective radon activity concentration in equilibrium of the respective source in this volume with the assigned uncertainty (k=1) is given by the values placed at the according positions. Fitting this model to the data points, results in a common calibration and a background reading factor for the detector. The difference between model and data is shown as residual in the lower graph.

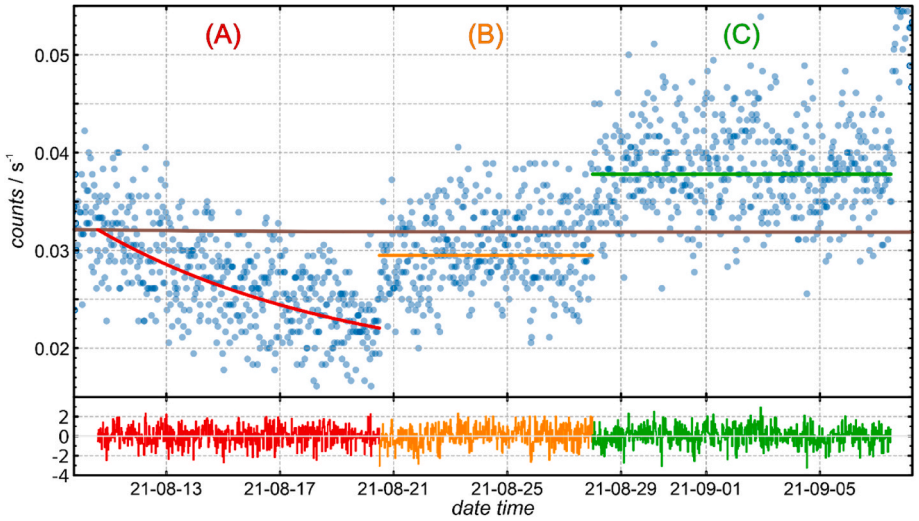

Fig. 11. Background determination methods during the calibration of a highly sensitive radon detector in a calibration chamber. The different colours indicate different radon suppression/reduction methods applied. (A) (red): flushing the calibration chamber with radon free aged, synthetic air. (B)(orange): cleaning calibration chamber air circulating it through an activated charcoal circle. (C)(green): closing the outer circulation loop of the detector, preventing radon to be sucked into the detectors active volume.

ANSTO 200 L monitor while shutting down the outer loop ventilation. The result is given in Fig. 11 and was included in the uncertainty budget for the calibration.

The respective reference activity concentration is calculated from the SI traceable activity of these sources, their emanation coefficient and the active volume. Corrections for a background activity concentration and a loss of activity concentration (in case of leakage) are implemented for purpose of the uncertainty. In all cases the model resulting the fit, giving consistency with the assumption that there is no loss of activity and that the intrinsic background reading is adding to the uncertainty below 1 % but it is important to note that these assumptions of the calculation model are valid (see Table 5).

The determination of the characteristic limits for the ANSTO 200 L monitor was performed according to ISO 11929:2012 in two ways: In a direct analytical calculation and by Monte Carlo simulation on the basis of the mathematical model for the calibration in the climate chamber (see Table 6).

This example proofs the usefulness and achievable low uncertainties of the newly developed emanation sources for the direct and SI traceable calibration of highly sensitive radon activity concentration monitors.

7. Summary and conclusion

The need to develop traceability for low radon activity concentrations has provided the impetus for a new technology for radionuclide sources with small or even very small activities. This step prepares the way for environmental measurements in the field with uncertainties on a scale not previously achieved: Although the measured quantity is now two orders of magnitude smaller, the uncertainties are comparable to those previously achieved in the medium activity range. This result represents a milestone for the development of measurement technology for atmospheric measurement of radon activity concentration.

Two large scientific communities, climate change observation and radiological protection will benefit from the development. In the combat against both climate change and radiation exposure, measurements must be supported by traceable metrology infrastructure providing reliable data for scientists and decision makers. The EMPIR 19ENV01 traceRadon[3] project supports the build-up of quality assured infrastructure in labs and in the field by which reliable data can be provided.

CRediT authorship contribution statement

Stefan Röttger: Writing – review & editing, Writing – original draft, Visualization, Validation, Supervision, Software, Resources, Project administration, Methodology, Investigation, Funding acquisition, Formal analysis, Data curation, Conceptualization. **Annette Röttger:** Writing – review & editing, Writing – original draft, Visualization,

Table 5
Final results for the calibration of a possible transfer standard for outdoor air ^{222}Rn activity concentration detectors, indicating the calibration factor, the sensitivity and the intrinsic background.

C Bq·m^{-3}	*u(C)* Bq·m^{-3}	*calibration factor k* s·Bq·m^{-3}	*sensitivity* k_c (s·Bq·m^{-3})$^{-1}$	*intrinsic background in the chamber* s^{-1}
7.76	0.13	26.0 ± 0.5	0.0385 ± 0.0013	0.03107 ± 0.00015
13.38	0.16			
18.09	0.17			
21.14	0.23			

[3] This project 19ENV01 has received funding from the EMPIR programme co-financed by the Participating States and from the Europe'n Union's Horizon 2020 research and innovation programme.

Table 6
Determined values of decision threshold and detection limit for a possible transfer standard, regarding different techniques and according to ISO 11929:2012.

calculation method	decision threshold Bq·m^{-3}	*detection limit* Bq·m^{-3}
MC simulation	0.26	0.55
quantity value	0.18	0.40
	7.76 ± 0.13	7.76 ± 0.13

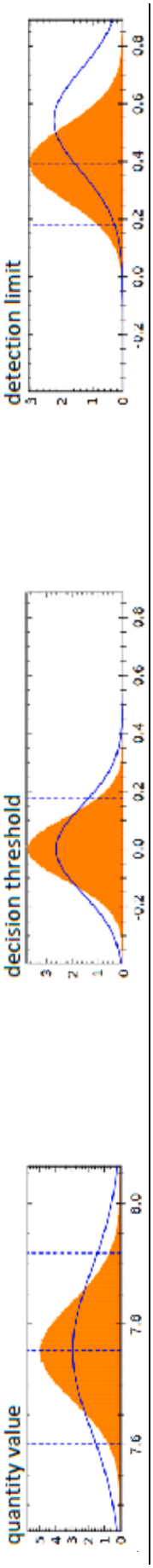

Validation, Supervision, Software, Resources, Project administration, Methodology, Investigation, Funding acquisition, Formal analysis, Data curation, Conceptualization. **Florian Mertes:** Visualization, Validation, Software, Methodology, Investigation, Formal analysis. **Viacheslav Morosch:** Visualization, Validation, Software, Methodology, Investigation, Formal analysis, Data curation. **Tanita Ballé:** Visualization, Validation, Investigation. **Scott Chambers:** Writing – review & editing, Methodology, Investigation, Data curation.

Declaration of competing interest

The authors declare the following financial interests/personal relationships which may be considered as potential competing interests: Annette Roettger reports financial support was provided by EURAMET European Metrology Programme for Innovation and Research.

Data availability

Data is shared open access and FAIR given in references but are also available on request.

Acknowledgements

EMPIR 19ENV01 traceRadon project was launched in summer 2020. It is supported by a broad global scientific community within climate research, radiation protection and metrology. All stakeholders are united by the goal of providing new and improved data for science, the public and decision makers. The consortium would like to thank the staff of project partners and collaborators of traceRadon, as well as all institutions and organisations that supported the project with recommendations.

References

Angell, W.J., 2009. WHO handbook on indoor radon: a public health perspective [Online]. Available: https://www.who.int/publications/i/item/9789241547673. (Accessed 12 May 2022).

Catherall, R., et al., 2017. The ISOLDE facility. J. Phys. G Nucl. Part. Phys. 44 (9), 094002 https://doi.org/10.1088/1361-6471/aa7eba.

Commission, E., Centre, J.R., 2020. European Atlas of Natural Radiation. Publications Office. https://doi.org/10.2760/46388.

Darby, S., et al., 2005. Radon in homes and risk of lung cancer: collaborative analysis of individual data from 13 European case-control studies. BMJ 330 (7485), 223. https://doi.org/10.1136/bmj.38308.477650.63.

Gesetz zur Neuordnung des Rechts zum Schutz vor der schädlichen Wirkung ionisierender Strahlung, Jun. 27, 2017. 1966 Bundesgesetzblatt Jahrgang 2017 Teil I Nr. 42. ausgegeben zu Bonn am 3. Juli 2017, vol. 1, no. 42. Bundesgesetzblat, pp. 1–102. Accessed: May 12, 2022. [Online]. Available: https://www.bgbl.de/xaver/bgbl/start.xav?startbk=Bundesanzeiger_BGBl&jumpTo=bgbl117s1966.pdf#__bgbl__%2F%2F*%5B%40attr_id%3D%27bgbl117s1966.pdf%27%5D__1652346311852.

Jörg, F., Eurin, G., Simgen, H., 2022. Production and characterization of a 222-Rn-emanating stainless steel source. Jan. 18, 2023. [Online]. Available: https://cds.cern.ch/record/2845390/files/INTC-P-647.pdf.

Kieck, T., Dorrer, H., Düllmann, C.E., Gadelshin, V., Schneider, F., Wendt, K., 2019. Highly efficient isotope separation and ion implantation of 163Ho for the ECHo project. Nucl. Instrum. Methods Phys. Res. 945, 162602. https://doi.org/10.1016/j.nima.2019.162602.

Linzmaier, D., Röttger, A., 2013. Development of a low-level radon reference atmosphere. Appl. Radiat. Isot. 81, 208–211. https://doi.org/10.1016/j.apradiso.2013.03.032.

Linzmaier, D., Röttger, A., 2014. Development of a transfer standard for the measurement of low Rn-222 activity concentration in air. Appl. Radiat. Isot. 87, 306–309. https://doi.org/10.1016/j.apradiso.2013.11.076.

Marouli, M., Pommé, S., van Ammel, R., García-Toraño, E., Crespo, T., Pierre, S., 2017. Direct measurement of alpha emission probabilities in the decay of 226 Ra. Appl. Radiat. Isot. 125, 196–202. https://doi.org/10.1016/j.apradiso.2017.04.029.

Mertes, F., Röttger, S., Röttger, A., 2019. A new primary emanation standard for Radon-222. Appl. Radiat. Isot. 156, 2020. https://doi.org/10.1016/j.apradiso.2019.108928.

Mertes, F., et al., 2022a. Ion implantation of ^{226}Ra for a primary ^{222}Rn emanation standard. Appl. Radiat. Isot. 181 https://doi.org/10.1016/j.apradiso.2021.110093.

Mertes, F., Röttger, S., Röttger, A., 2022b. Development of ^{222}Rn emanation sources with integrated quasi 2π active monitoring. Int. J. Environ. Res. Publ. Health 19 (2). https://doi.org/10.3390/ijerph19020840.

Picolo, J.L., 1996. Absolute measurement of radon 222 activity. Nucl. Instrum. Methods Phys. Res., Sect. A 369 (2–3), 452–457.

Rat der europäischen Kommission (EK), 2013. Richtlinie 2013/59/EURATOM des Rates vom 5. Dezember 2013 zur Festlegung grundlegender Sicherheitsnormen für den Schutz vor den Gefahren einer Exposition gegenüber ionisierender Strahlung und zur Aufhebung der Richtlinien 89/618/Euratom, 90/641/Euratom, 96/29/Euratom, 97/43/Euratom und 2003/122/Euratom. EU [Online]. Available: https://www.base.bund.de/SharedDocs/Downloads/BASE/DE/rsh/1f-recht-eu/1F-2-1-RL-2013-59-kons2016de.pdf;jsessionid=809A144C085F83AEACE5ABD6B10FD11F.1_cid374?__blob=publicationFile&v=1. (Accessed 12 May 2022).

Röttger, S., Paul, A., Honig, A., Keyser, U., 2001. On-line low- and medium-level measurements of the radon activity concentration. Nucl. Instrum. Methods Phys. Res. 466 (3) https://doi.org/10.1016/S0168-9002(01)00227-3.

Röttger, S., et al., 2022a. Radon metrology for use in climate change observation and radiation protection at the environmental level. Adv. Geosci. 57, 37–47. https://doi.org/10.5194/adgeo-57-37-2022.

Röttger, S., Röttger, A., Mertes, F., 2022b. IRSD Raw Alpha Spectrum Data for Rn-222 Emanation Determination. Physikalisch-Technische Bundesanstalt, Braunschweig. https://doi.org/10.7795/720.20220921.

Röttger, S., Röttger, A., Mertes, F., 2023. In: Calibration of a ANSTO 200 L Detector Using Rn-222 Emanation Sources. Physikalisch-Technische Bundesanstalt, Braunschweig Jan. 20, doi: 10.7795/720.20230119.

Further readings

Chambers, S.D., et al., 2016. Towards a universal 'baseline' characterisation of air masses for high- and low-altitude observing stations using radon-222. Aerosol Air Qual. Res. 16 (3), 885–899. https://doi.org/10.4209/aaqr.2015.06.0391.

Chambers, S.D., et al., 2018. Characterizing atmospheric transport pathways to Antarctica and the remote southern ocean using radon-222. Front. Earth Sci. 6 https://doi.org/10.3389/feart.2018.00190.

Chambers, S., et al., 2019. Skill-testing chemical transport models across contrasting atmospheric mixing states using radon-222. Atmosphere 10 (1), 25. https://doi.org/10.3390/atmos10010025.

Melintescu, A., Chambers, S.D., Crawford, J., Williams, A.G., Zorila, B., Galeriu, D., 2018. Radon-222 related influence on ambient gamma dose. J. Environ. Radioact. 189, 67–78. https://doi.org/10.1016/j.jenvrad.2018.03.012.

Zhang, B., et al., 2021. Simulation of radon-222 with the GEOS-Chem global model: emissions, seasonality, and convective transport. Atmos. Chem. Phys. 21 (3), 1861–1887. https://doi.org/10.5194/acp-21-1861-2021.